EARTHQUAKES; forecasting and prediction.

Why have we failed?

NEED: Observation-driven modeling!

Selwyn Sacks,

with Paul Rydelek, Debbie Smith, Kiyoshi Suyehiro

- Propose an idea of long-term evaluation and show why we now focus on the Tokai segment
- Propose an idea for forecasting and prediction and suggest the need to monitor the aquifer. (Vertical component strainmeter?)
- Concluding remarks

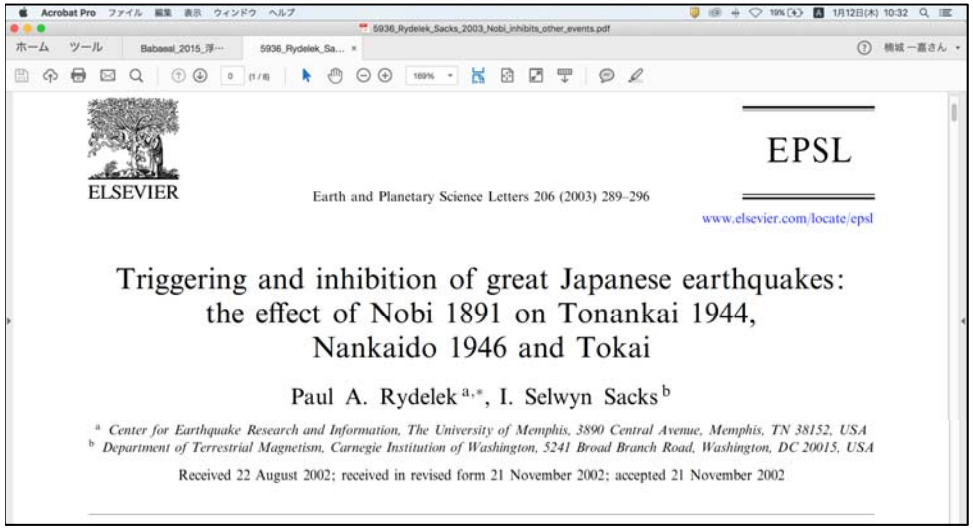

ELSEVIER

EPSL

Earth and Planetary Science Letters 206 (2003) 289–296

www.elsevier.com/locate/epsl

Triggering and inhibition of great Japanese earthquakes: the effect of Nobi 1891 on Tonankai 1944, Nankaido 1946 and Tokai

Paul A. Rydelek [a,*], I. Selwyn Sacks [b]

[a] *Center for Earthquake Research and Information, The University of Memphis, 3890 Central Avenue, Memphis, TN 38152, USA*
[b] *Department of Terrestrial Magnetism, Carnegie Institution of Washington, 5241 Broad Branch Road, Washington, DC 20015, USA*

Received 22 August 2002; received in revised form 21 November 2002; accepted 21 November 2002

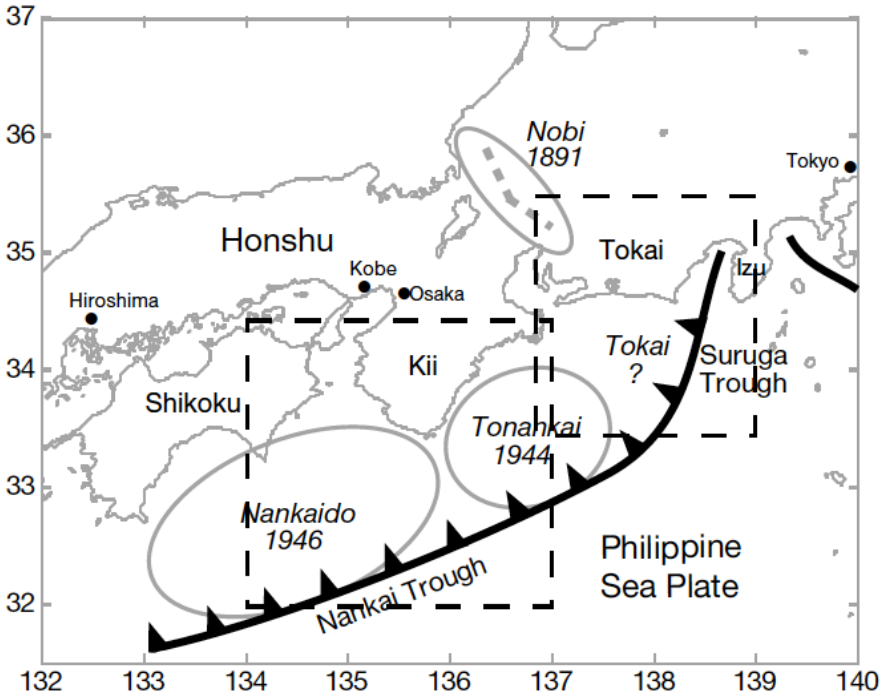

Fig. 1. Map of southwest Japan showing the Nankai and Suruga Troughs and the rupture zones of the Nankaido 1944, Tonankai 1946, and Nobi 1891 earthquakes. These great events are caused by the subduction of the Philippine Sea plate beneath central and south Honshu at the rate of 4 cm/yr in the direction N 50°W. Modeling suggests that the time of occurrence of the mid-1940 earthquakes and the extent of rupture may have been influenced by stress changes due to postseismic strain diffusion following the great Nobi earthquake in 1891. The dashed boxes are areas used in Fig. 3 to show the effects of stress diffusion.

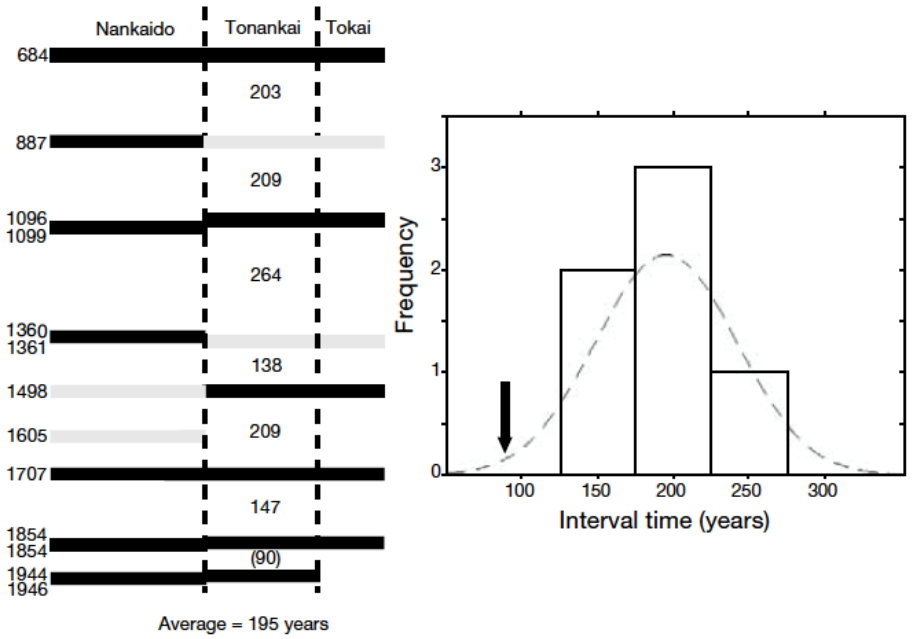

Fig. 2. (Left panel) Time–distance diagram of the largest earthquakes in the Nankai and Suruga Troughs since 684 AD. The Nankaido, Tonankai and Tokai sections of the subduction zone are shown in Fig. 1. The left column gives the year of the event and the horizontal bars show the extent of rupture. Gray bars indicate that evidence is from seismo-archeological studies and may be somewhat uncertain. The seismic shaking from the 1605 event was rather small and the extent of rupture is unknown but it was a tsunami producing earthquake. Recurrence times for Tonankai earthquakes are shown between bars; the average of 195 years excludes the 1944 event. (Right panel) Histogram of recurrence times for Tonankai earthquakes. The interval time preceding the 1944 earthquake (arrow) is much earlier than the mean of the histogram. The dashed line is a Gaussian fit to the data, albeit for an admittedly small population size.

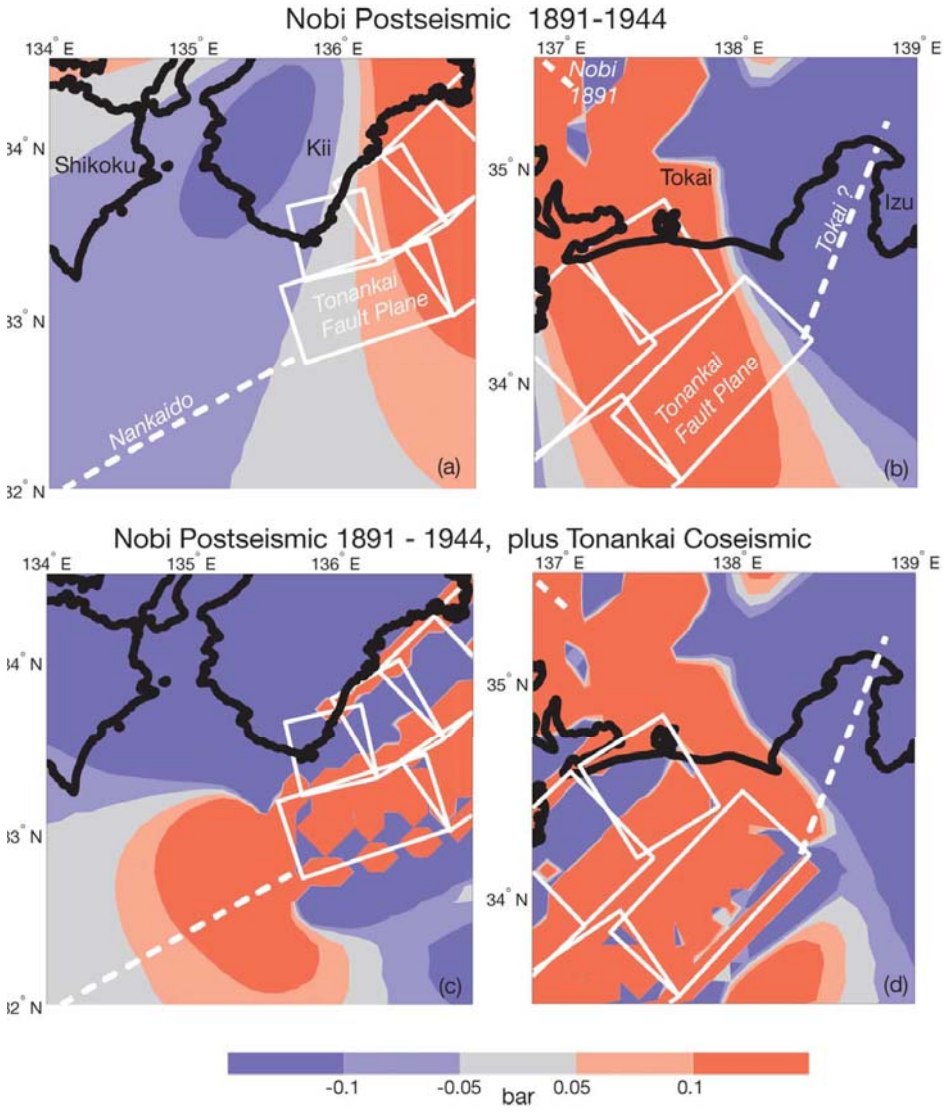

Fig. 3. Plots (a) and (b) are the dashed boxes in Fig. 1 showing the effects of viscoelastic postseismic relaxation in 1944 from the great inland Nobi earthquake in 1891. White dashed lines are the extensions of the Tonankai fault into Nankaido (west) and Tokai (east). The colored contours show increasing (red) and decreasing (blue) Coulomb failure stress in bars at a depth of ~10 km on shallow dipping (25°) planes that are parallel to the dashed lines in each figure. The white tiles representing the segments of the fault plane used to model the Tonankai earthquake are from Sagiya and Thatcher [23]; the easternmost segments are poorly constrained. Plots (c) and (d) include the coseismic effects from the 1944 Tonankai earthquake, determined from elastic theory [22] and the given fault model [23]. Postseismic effects follow the modeling of Pollitz and Sacks [8].

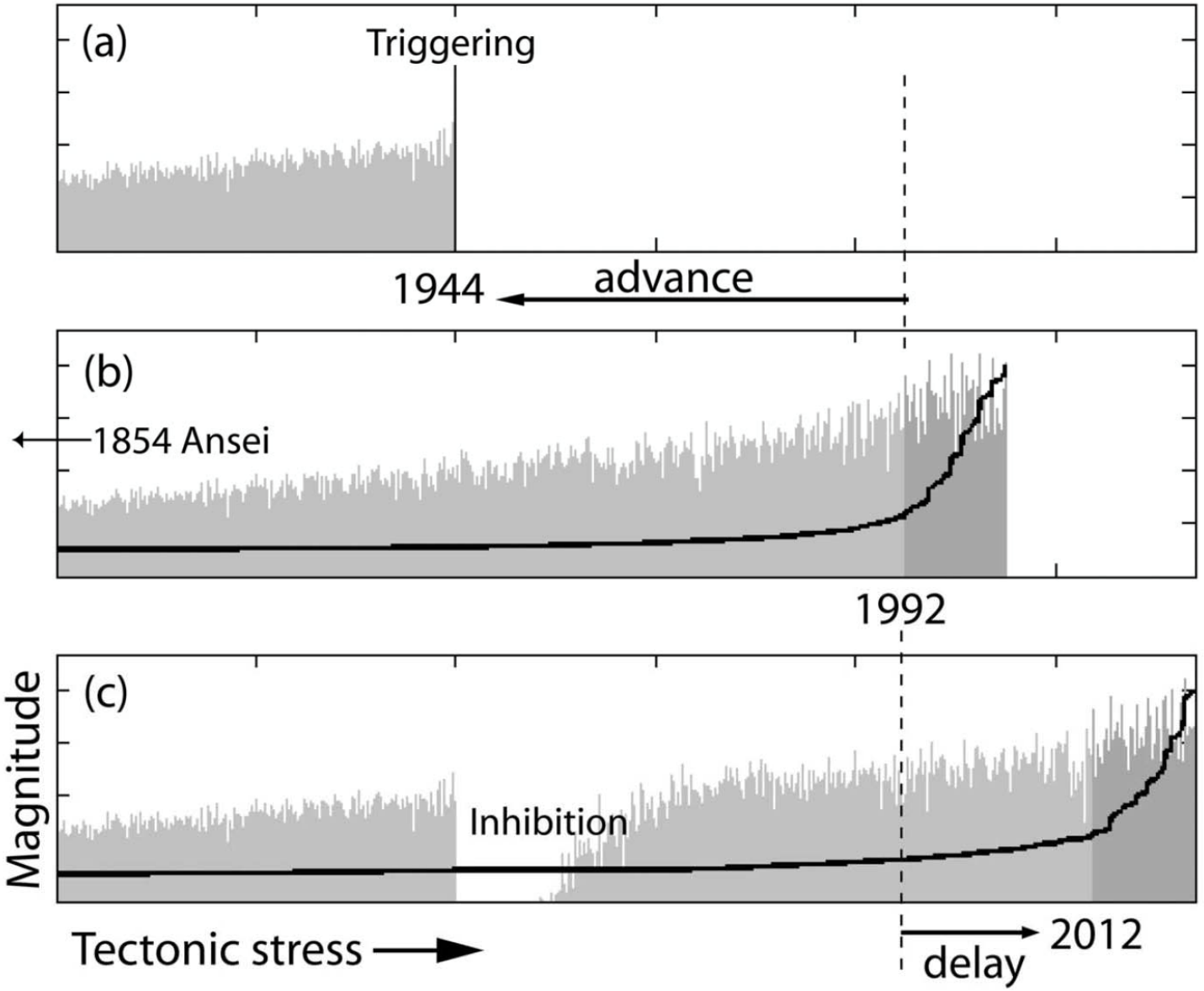

Fig. 4. Model results for triggering and inhibition of seismicity from a numerical simulation of the earthquake process [24,25]. In (b) the buildup of tectonic stress from the subduction of the Philippine Sea plate eventually results in failure of the fault. The thick black line shows the equivalent energy being released in the earthquake process, which is found to increase sharply when large-scale failure is imminent. The unperturbed time of failure is assumed to be 1992; this is the sum of the times since the last rupture in 1854 and the shortest previous repeat time of 138 years. In (a), postseismic stress from viscoelastic relaxation after the 1891 Nobi earthquake perturbs the fault and acts to trigger the Tonankai section in 1944. In (c), the postseismic perturbation, which is also applied in 1944, inhibits the Tokai section of the fault and delays the earthquake until 2012.

Cellular model.

To our surprise: gave

b-value ~ 1.

Varying slip concentration, space and time.

Stress drop << rock strength

More surprise; forecast of impending great earthquake!

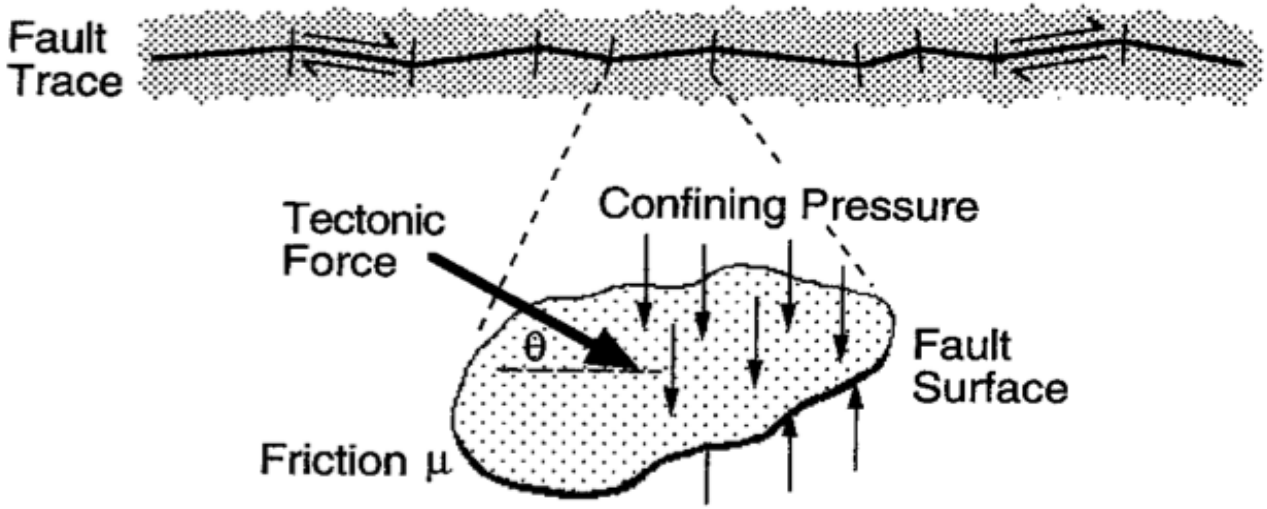

$$T\cos(\theta) \geqq \mu[T\sin(\theta) + P],$$

P is confining pressure minus pore pressure.

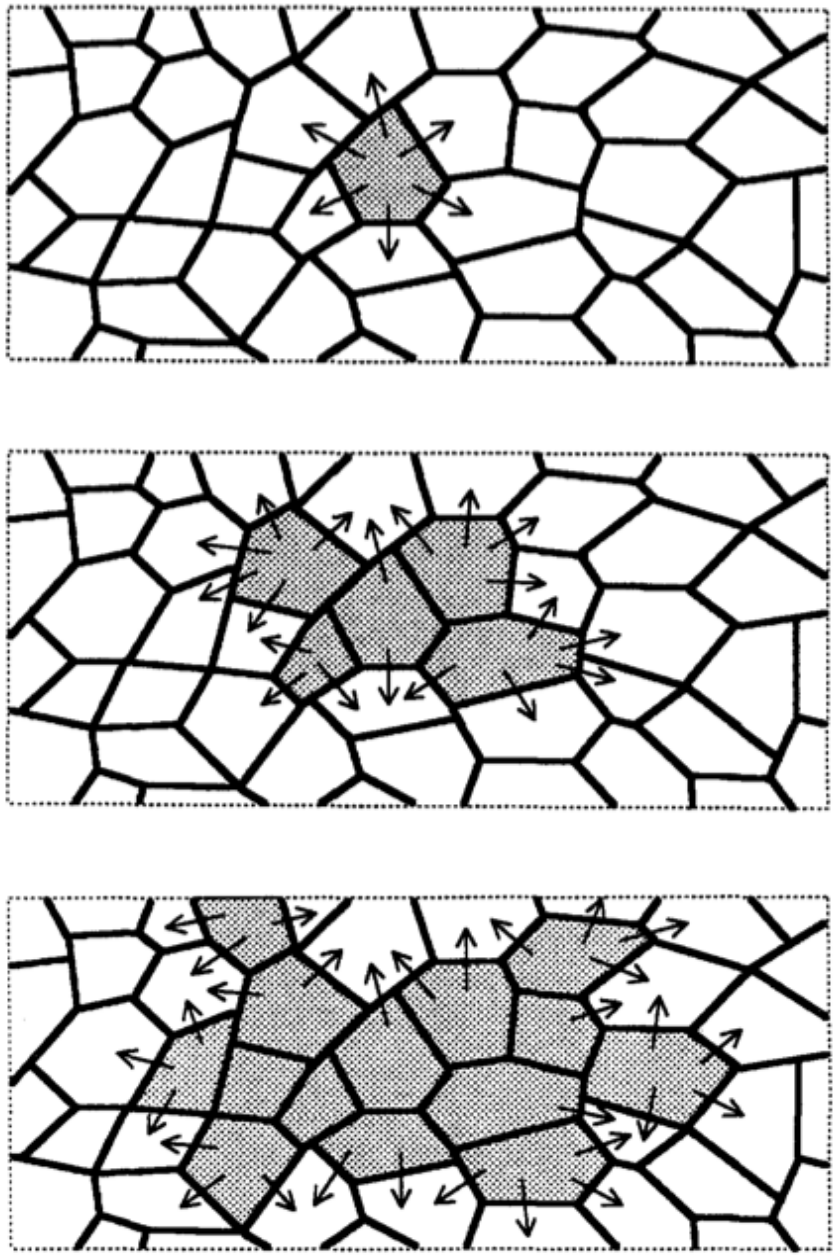

Figure 1. The concept of the quantum earthquake model is shown in this drawing. The fault plane is assumed to consist of patches, or quanta, that have somewhat different failure criteria. The loading and failure conditions are nearly constant over the surface of each quantum, which results in total failure on that surface when the Coulomb strength is exceeded. Upon failure of any quantum, such as the one at the center of the figure, a redistribution of stress occurs that may produce failure in neighboring quanta. This cascade process will continue until the stress redistribution is insufficient for further failure. Thus, the evolution of the earthquake process depends not only on the failure parameters in the model but also on the history of seismicity.

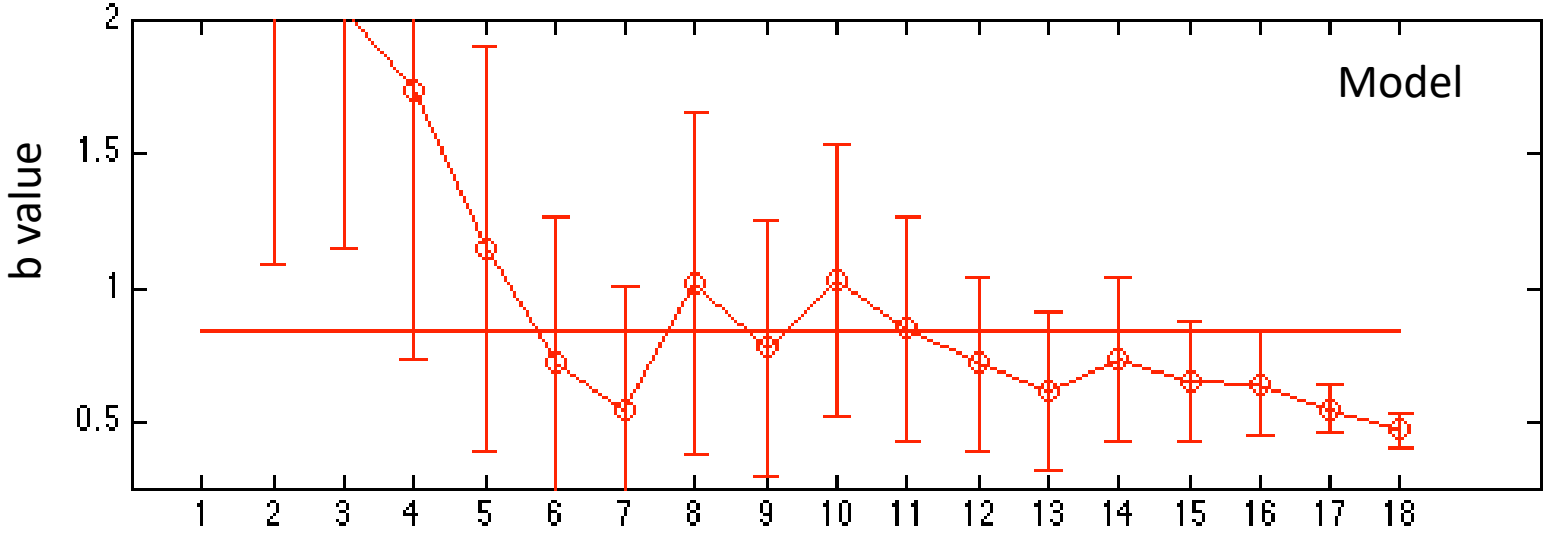
Model
b value
2
1.5
1
0.5
1 2 3 4 5 6 7 8 9 10 11 12 13 14 15 16 17 18

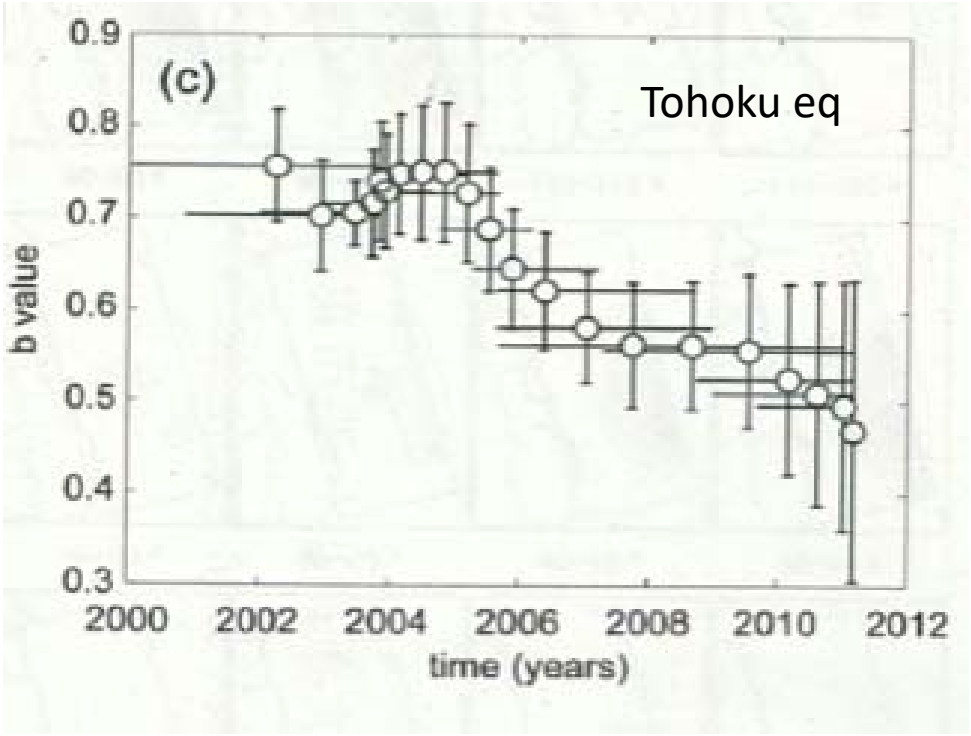
(c)
Tohoku eq
b value
0.9
0.8
0.7
0.6
0.5
0.4
0.3
2000 2002 2004 2006 2008 2010 2012
time (years)

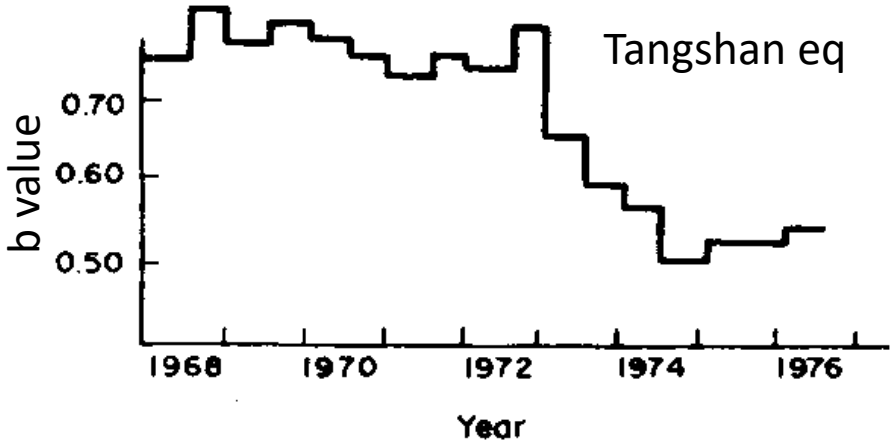
Tangshan eq
b value
0.70
0.60
0.50
1968 1970 1972 1974 1976
Year

- Water and dilatancy.
- Fault strength effected by pore pressure.
- Rock strength increases with dilatancy. (Rice 1975)
- Shear stress on rock increases rock volume (slightly)

- Magnitude-dependent quiescence.

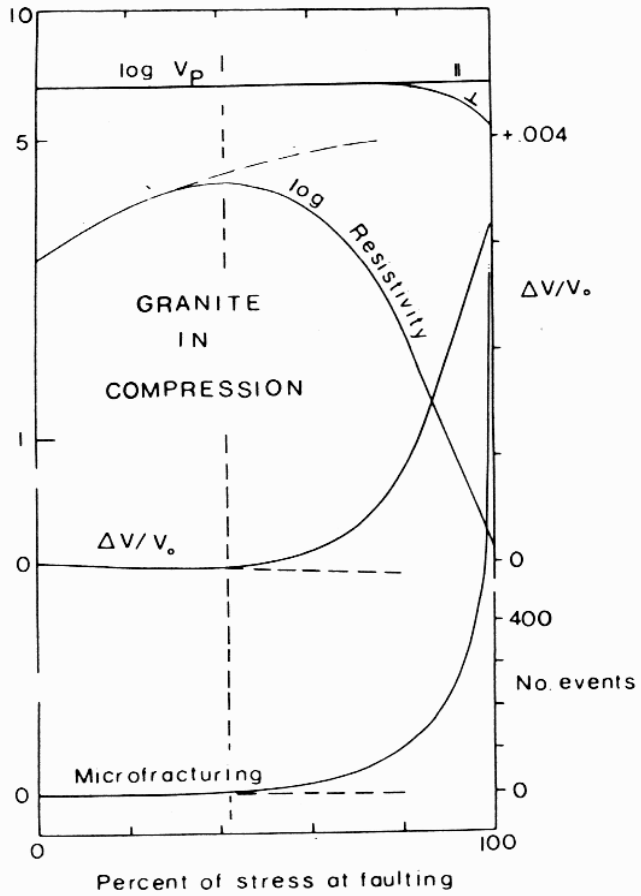

Fig. 13-1. Changes in the physical properties of granite with compr for Westerly granite under several kilobars confining pressure (Brace, ing data are from Scholz (1967).

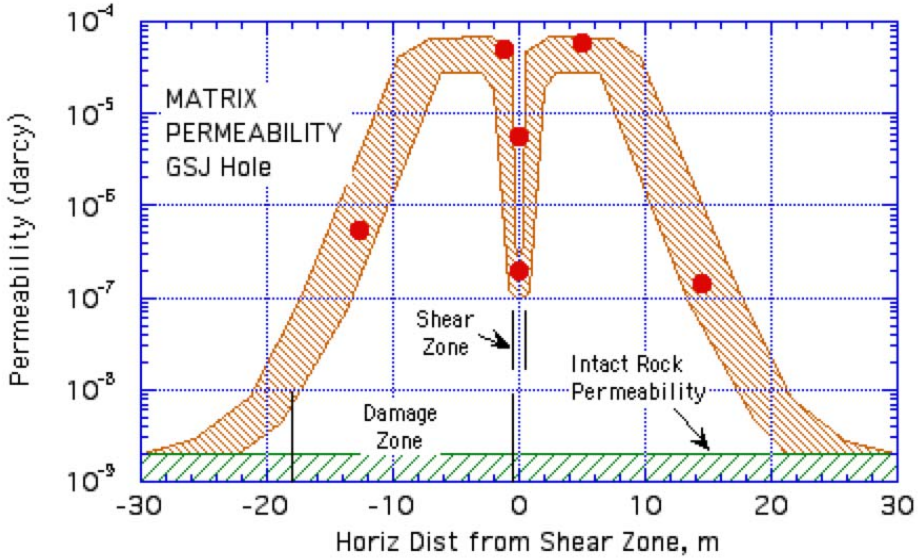

Figure 5. Profile of matrix permeability for the GSJ hole measured at 50 MPa confining pressure. The low permeability shear zone is surrounded by a high permeability damage zone.

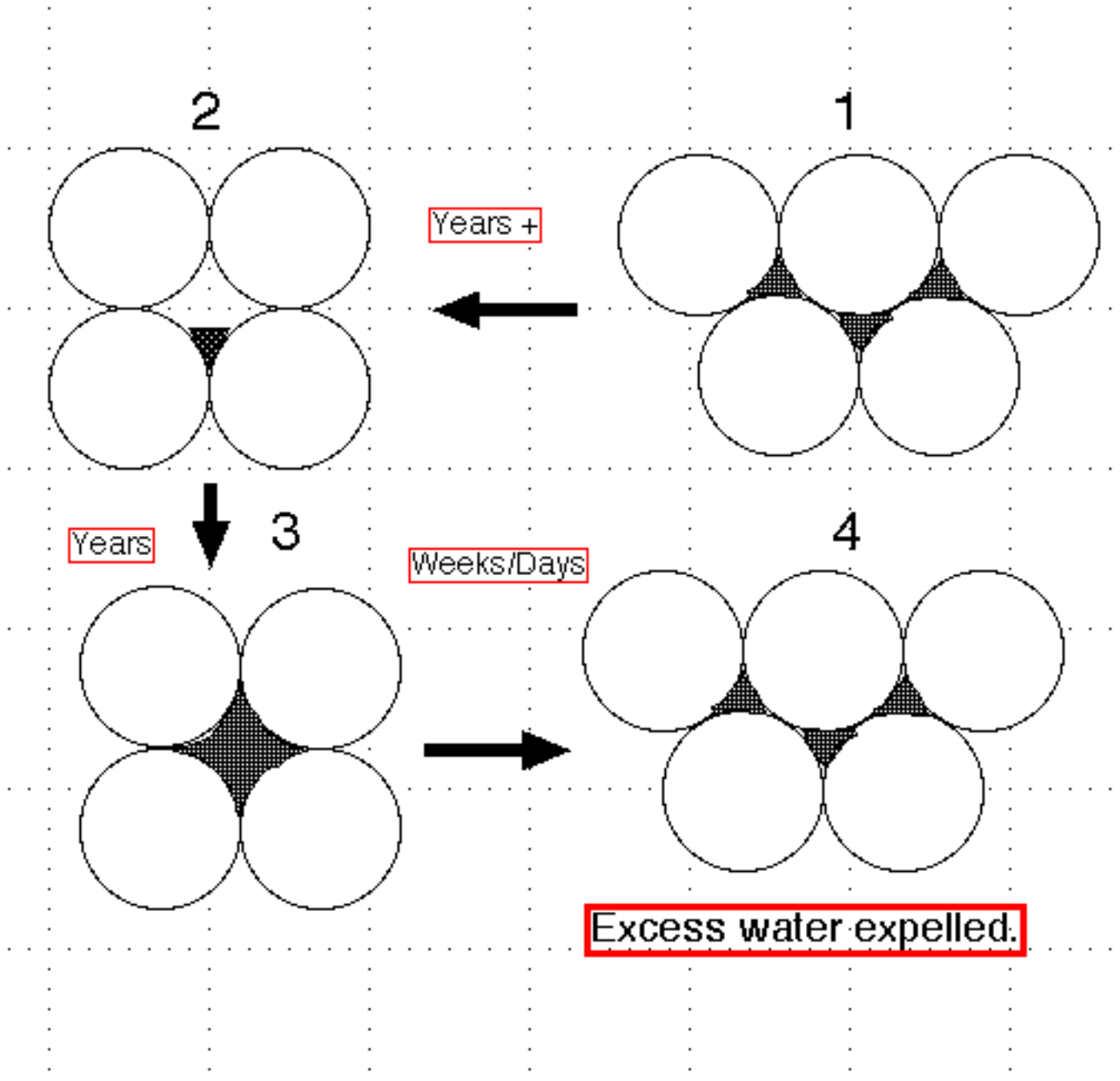
2
1
Years +
Years
3
Weeks/Days
4
Excess water expelled.

Quiescence Before the Urakawa-Oki Earthquake

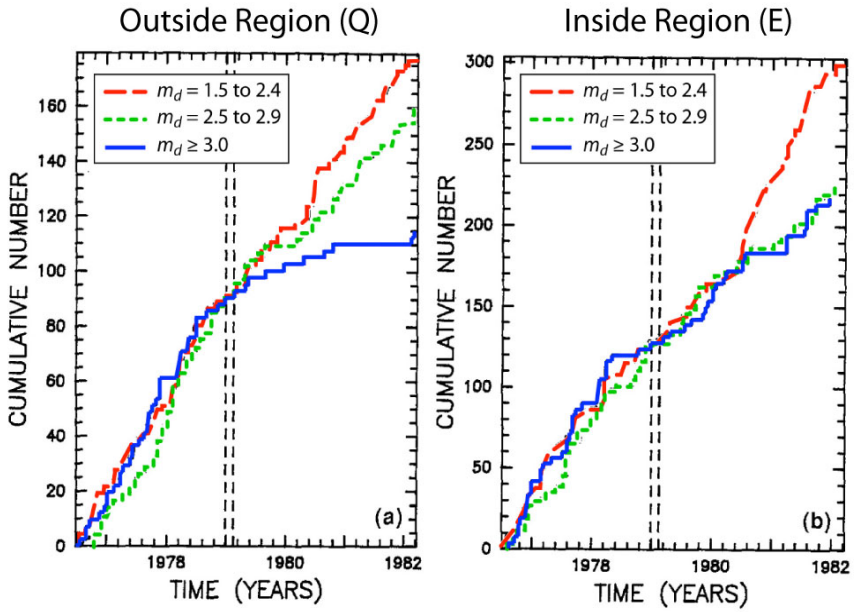

(Modified from Taylor *et al.*, 1991)

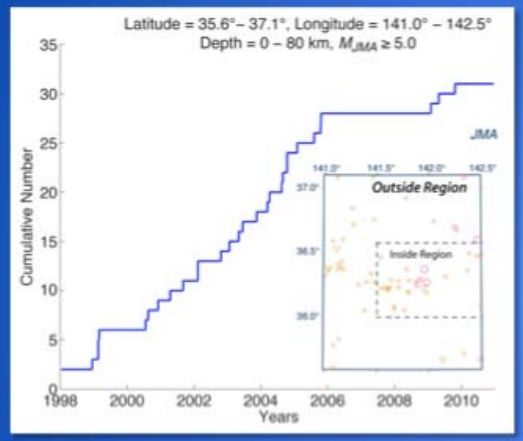

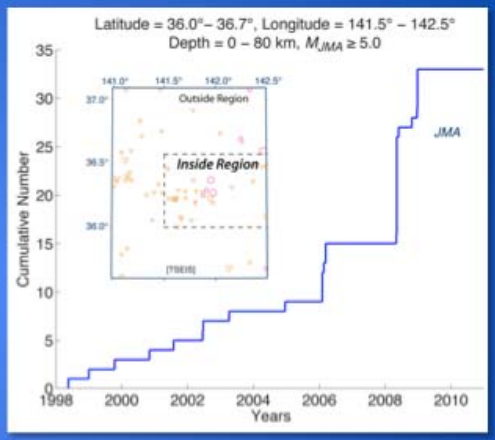

- Quiescence is seen for large events in the Outside Region prior to the March 11, 2011 Tohoku-Oki event.
- Activation is seen at a slightly later time in the Inside Region

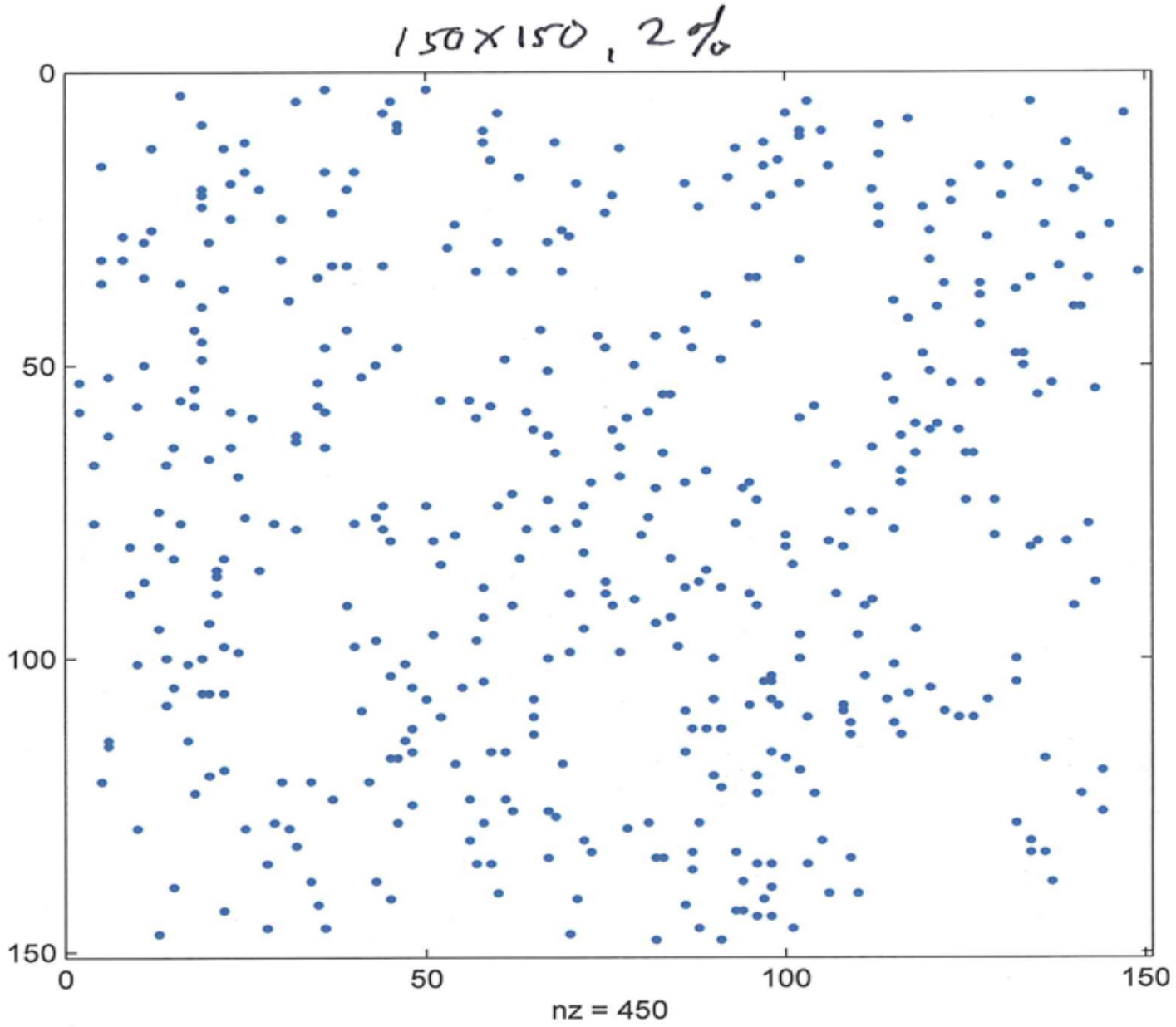
150×150, 2%
0
50
100
150
0
50
100
150
nz = 450

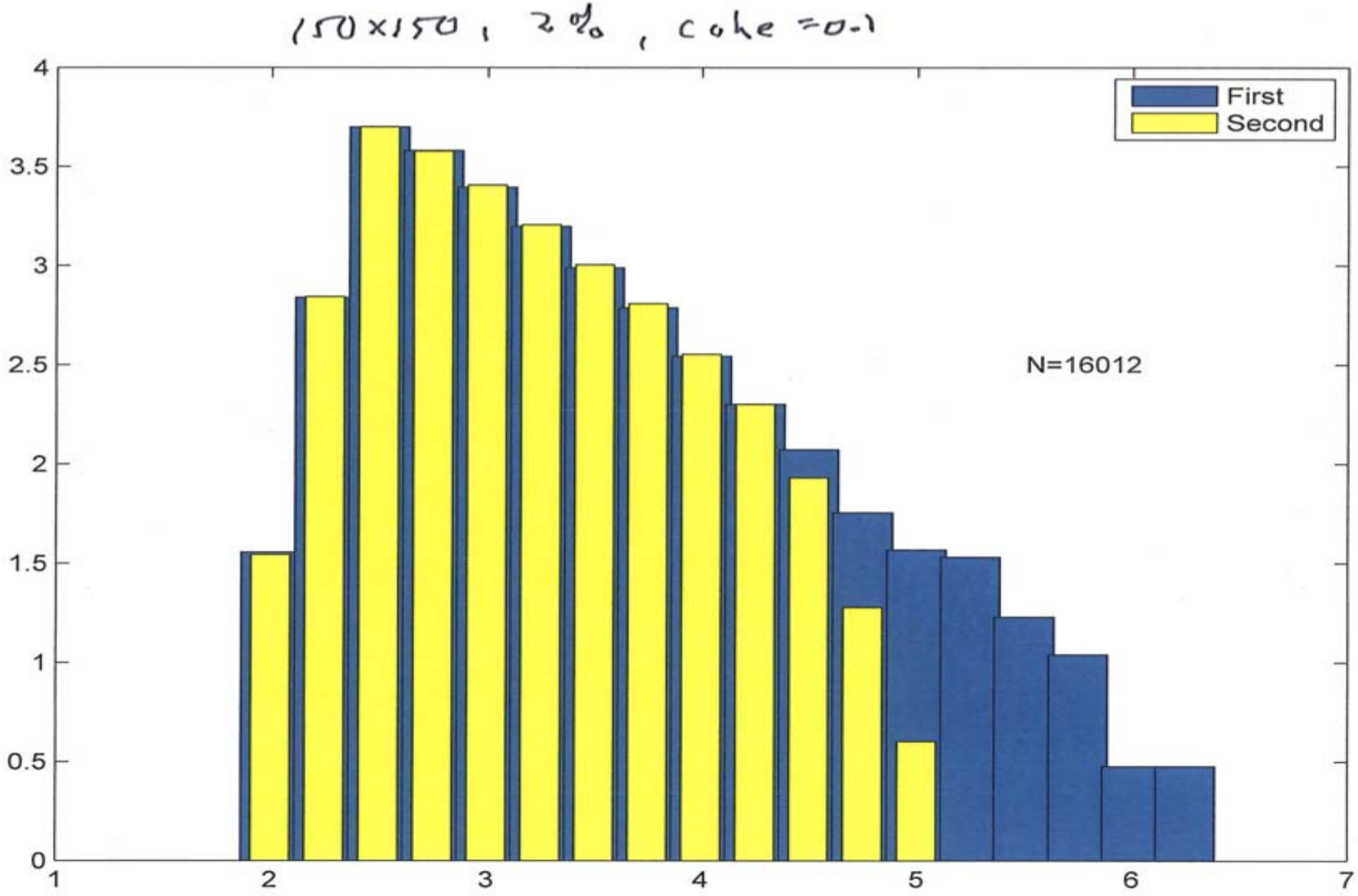
150x150, 2%, coke=0.1
First
Second
N=16012
4
3.5
3
2.5
2
1.5
1
0.5
0
1
2
3
4
5
6
7

For Forecast/Prediction:

b-value for very large earthquakes only because the eventual location is not well known.

Quiescence region of m>3+ in high stress regions is much larger than the fault zone so is easier to recognize.

These are Forecasts only, time within years.

Dilatancy collapse gives a chance for prediction (days/weeks)

- Note that magnitude-dependent quiescence relies on the long duration of the stiffened dilatant zone, since the seismic observations that identify this zone take weeks to years to establish this behavior. This of course would be the case in the rock outside the fault zone itself.
- However, in the fractured fault zone, the high permeability will allow the dilatant regions to refill so reducing the failure strength. Therefore there should be no quiescent region in the fault region.

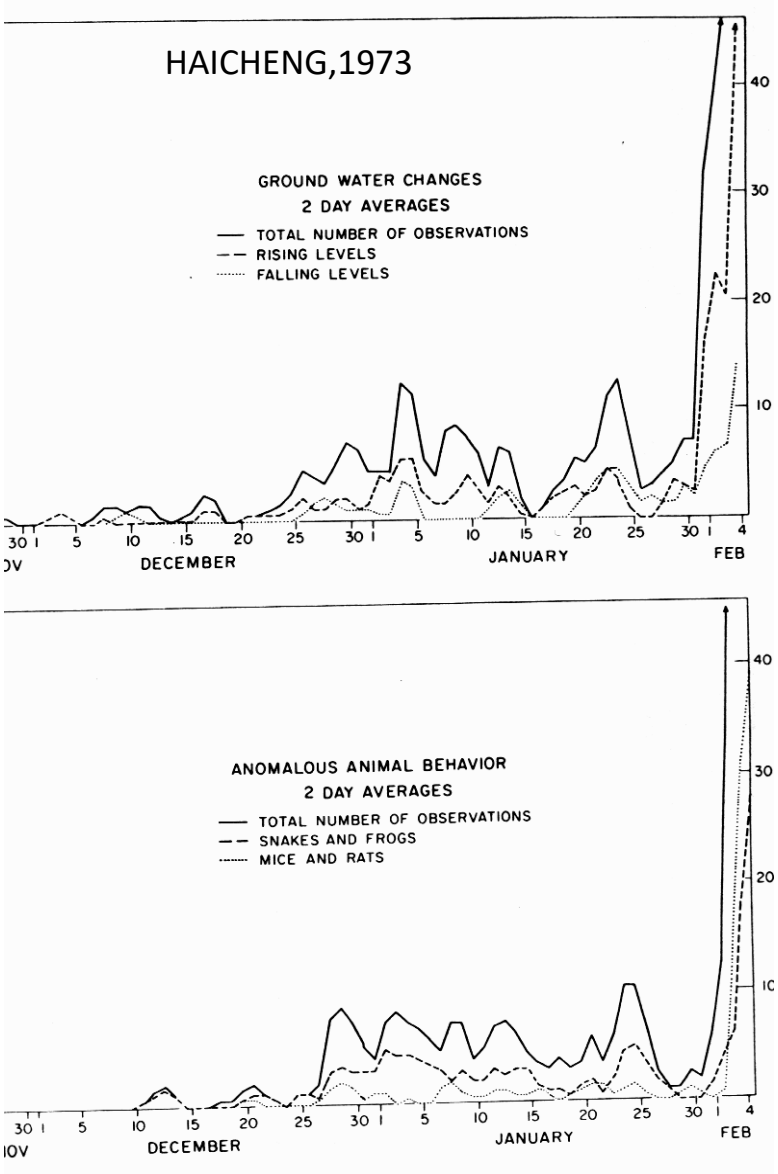

ig. 6. Two-day averages made daily of the data
in Fig. 5.

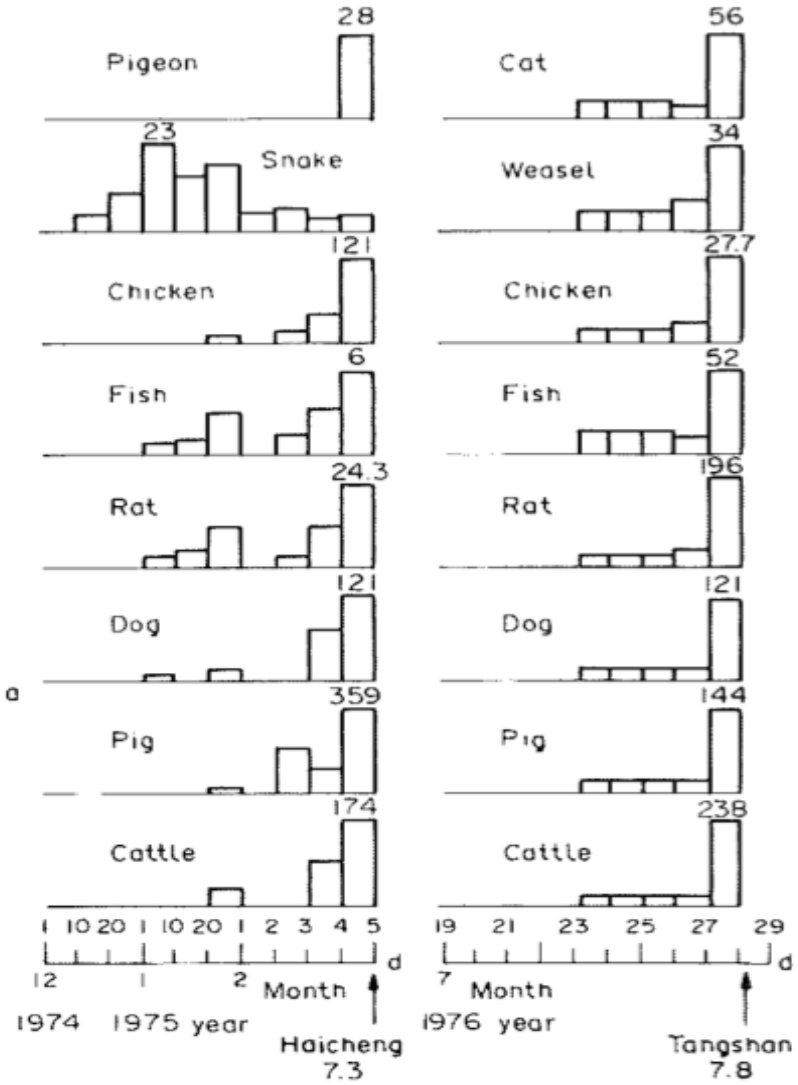

FIGURE 4.13 Comparison of the number of anomalous animal behaviour reports before the Haicheng and Tangshan earthquakes. The data for Haicheng are for the 1 December, 1974 to 5 February, 1975, and the data for Tangshan are for the period 19 to 29 July, 1976. Note that the former had anomalies occurring as early as 1–2 months before the shock, whereas the latter had appreciable anomalies only 2 days before the main shock.

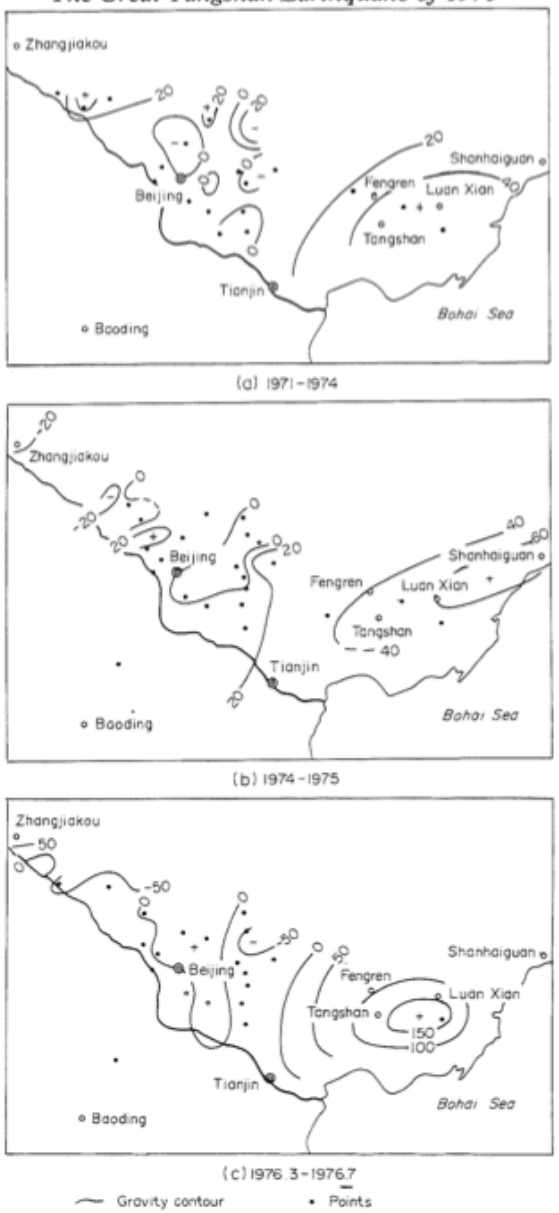

FIGURE 3.19 Variation of gravity (in 10^{-8} cm/s^2) in Beijing–Tianjin–Tangshan–Zhangjiakou region from 1974 through 1976. [a] Yearly average for 1971 till 1974; [b] yearly average for 1974 till 1975; [c] total gravity change for the period March to July of 1976.

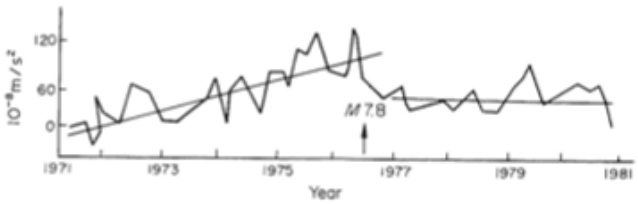

FIGURE 3.20 Gravity change measured at Station I in Tangshan. Note it increased continually for about 3 years prior to the Tangshan earthquake when it peaked off, and then rebounded after the event.

with three to five duplicate measurements each time. The daily average was used to track the resistivity change.

It can be seen from Figure 3.21 that the overall trend was for the

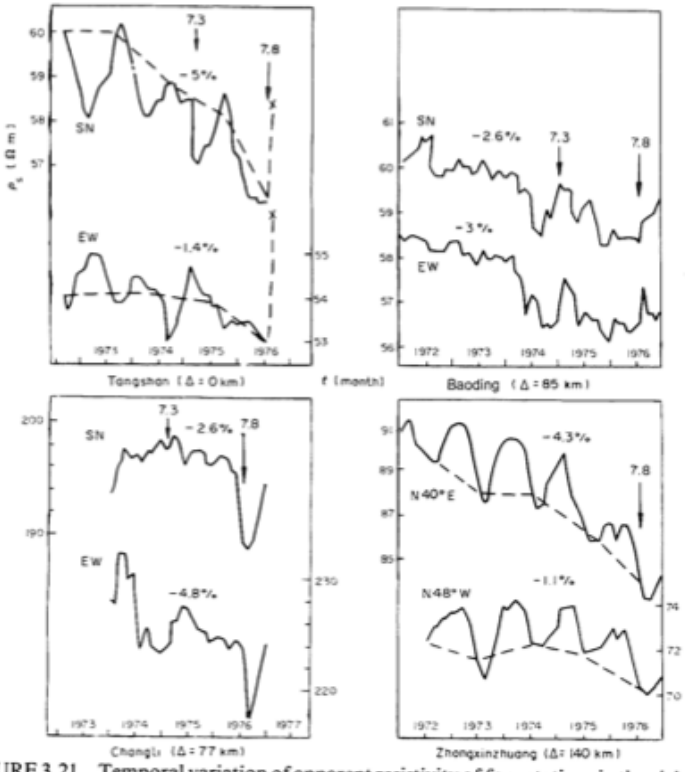

FIGURE 3.21 Temporal variation of apparent resistivity of four stations in the vicinity of Tangshan. (After Qian, J. *et al.*, in *Earthquake Prediction*, Proc. 1979 UNESCO Symposium, Terrapub, 1984.)

apparent electrical resistivity to decrease before the 1976 earthquake. This trend of a temporal decrease in resistivity lasted for 2–3 years and reversed itself after the main shock.

Wenchuan earthquake, m~8, 12 May 2008.

Precursory animal behavior and water level (springs etc) change.

Rates:

Period: Jan 01 – April 30th.	1/day
May 01 - May 7	25
May 8 - May 11	80
May 12	198

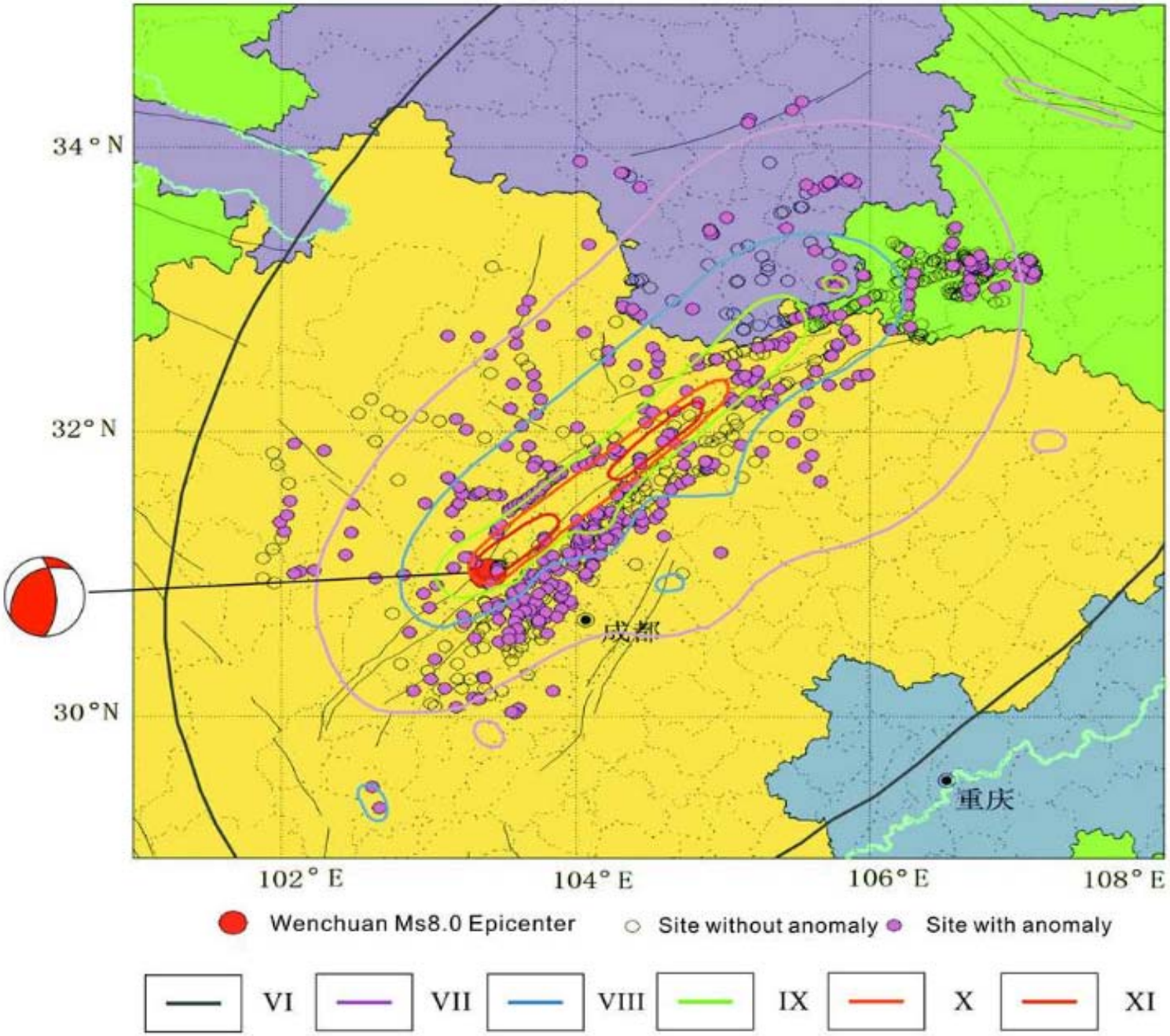
34° N
32° N
30° N
102° E
104° E
106° E
108° E
成都
重庆
Wenchuan Ms8.0 Epicenter
Site without anomaly
Site with anomaly
VI
VII
VIII
IX
X
XI

Best-year production variability map of Barnett Shale Horizontal Wells

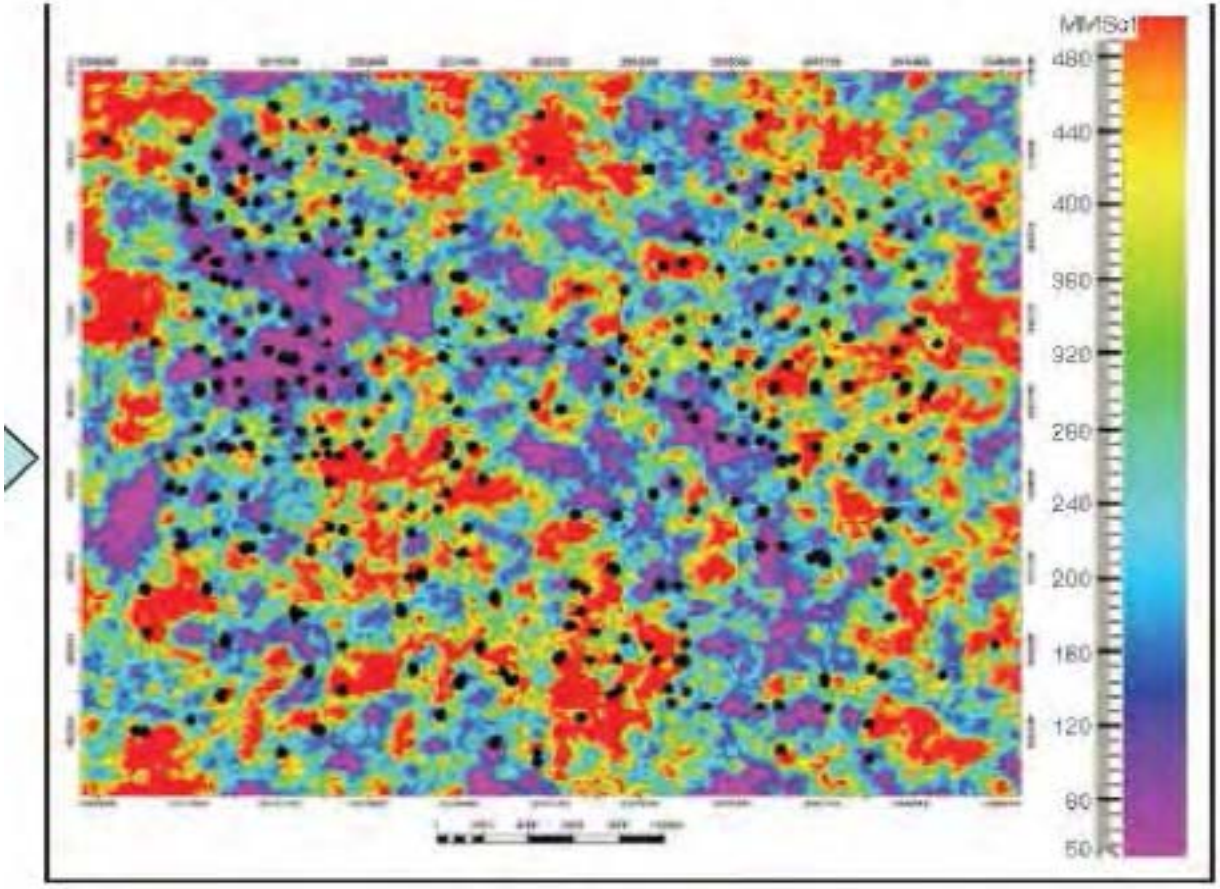

Summary. For Earthquake prediction.

- We may only have two weeks or less.
- Need to monitor the aquifer. (Vertical component strainmeter?)
- Bureaucracy approach change.